

Efficient Micro-Lasers Based on Highly-Doped Monoclinic Double Tungstates

Xavier Mateos, Pavel Loiko, Josep Maria Serres, Konstantin Yumashev, Uwe Griebner, Valentin Petrov, Magdalena Aguiló and Francesc Díaz

Abstract— We demonstrate the suitability of monoclinic double tungstates (MDTs), $KRE(WO_4)_2$ where RE = Gd, Y or Lu, doped with Nd^{3+} , Yb^{3+} , Tm^{3+} or Ho^{3+} ions and co-doped with Yb^{3+} - Tm^{3+} or Tm^{3+} - Ho^{3+} ion couples, for highly-efficient micro-lasers at ~ 1 μm and at ~ 2 μm . This is facilitated by the use of high rare-earth doping levels (up to 15 at.% for Tm, 10 at.% for Nd and 25 at.% for Yb) and a special crystal cut along the N_g -axis providing the thermal guiding. Record slope efficiencies for bulk MDT lasers are achieved for each studied ion. A 15 at.% Tm:KLu(WO_4)₂ laser generated 785 mW at 1957...1965 nm with a slope efficiency $\eta = 77\%$. The quantum efficiency for Tm^{3+} ions amounted to $\eta_q = 1.98 \pm 0.02$. With a 0.9 mm-thick 25 at.% Yb:KLuW micro-laser, $\eta = 91\%$ is achieved, approaching the theoretical limit set by the Stokes shift.

Index Terms— Solid-state lasers, Monoclinic double tungstates, Micro-lasers, Yb, Tm, Ho, Nd.

I. INTRODUCTION

A microchip laser consists of a solid state active medium (AM) placed in a compact plano-plano cavity without air gaps [1]. Optionally, a saturable absorber (SA) can be integrated for pulsed operation [2]. The cavity mirrors can be directly deposited on the surfaces of the optical elements resulting in a monolithic set-up [3-5]. The microchip concept typically provides low intracavity losses, a robust and

Manuscript received December X, 2016. This work was supported by the Spanish Government under projects MAT2016-75716-C2-1-R, (AEI/FEDER,UE), MAT2013-47395-C4-4-R and TEC2014-55948-R, and by the Generalitat de Catalunya under project 2014SGR1358. F.D. acknowledges additional support through the ICREA academia award 2010ICREA-02 for excellence in research. This work is part of a project that has received funding from the European Union's Horizon 2020 Research and Innovation Program under the Marie Skłodowska-Curie grant agreement No 657630. P.L. acknowledges financial support from the Government of the Russian Federation (Grant 074-U01) through ITMO Post-Doctoral Fellowship scheme.

X. Mateos, J.M. Serres, M. Aguiló and F. Díaz are with Física i Cristal·lografia de Materials i Nanomaterials (FiCMA-FiCNA), Universitat Rovira i Virgili (URV), Campus Sescelades, c/ Marcel·lí Domingo, s/n., E-43007 Tarragona, Spain (e-mail: xavier.mateos@urv.cat; jserrese@gmail.com; magdalena.aguiló@urv.cat, f.diaz@urv.cat).

P. Loiko is with ITMO University, Kronverkskiy pr., 49, Saint-Petersburg, 197101, Russia (e-mail: kinetic@tut.by).

K. Yumashev is with the Center for Optical Materials and Technologies, Belarusian National Technical University, 65/17 Nezavisimosti Ave. 220013 Minsk, Belarus (e-mail: k.yumashev@tut.by).

X. Mateos, V. Petrov and U. Griebner are with the Max-Born-Institute for Nonlinear Optics and Short Pulse Spectroscopy, 2A Max-Born-Str., D-12489 Berlin, Germany (e-mail: mateos@mbi-berlin.de; petrov@mbi-berlin.de; griebner@mbi-berlin.de).

insensitive to misalignment set-up and, hence, high laser efficiency. Passively Q-switched microchip lasers are capable of generating very short (sub-ns) pulses [6-8] due to greatly reduced cavity roundtrip time and easy bleaching of the saturable absorber at the small size of the laser mode.

According to the theory of laser resonators, a plano-plano cavity is unstable unless it contains an intracavity focusing element [9]. Because optical pumping of the AM results in the formation of a thermal lens, it can stabilize the microchip laser cavity if the lens is positive (focusing) [10]. This mechanism is called thermal guiding and it is dominant for the microchip design. Other mechanisms, e.g. gain (index) guiding, thermal curvature of the crystal surfaces (end-bulging, which can be treated as a partial effect of the thermal lensing), or shaping of the crystal surfaces, exist but they are less common. The pump intensity dependence of the thermal lens [11] is typically a drawback in long laser cavities which can become unstable at a certain pump level. However, with the increase of pump power and, hence, optical (refractive) power of the positive thermal lens, the microchip cavity becomes even more stable [10]. Thus, besides the high absorption and stimulated-emission cross-sections required to achieve low laser threshold and high pump efficiency, an important criterion for the AM choice in microchip lasers is that it shows positive thermal lens.

From the point of view of the spectroscopic properties, the monoclinic double tungstates [12] (MDTs) with chemical formula $KRE(WO_4)_2$ or shortly KREW where RE stands for optically “passive” ions like Gd^{3+} , Y^{3+} or Lu^{3+} , doped with laser-active trivalent rare-earth ions (RE^{3+}), Yb^{3+} , Nd^{3+} , Tm^{3+} or Ho^{3+} , are very suitable for microchip lasers at ~ 1 and ~ 2 μm . They exhibit strong optical anisotropy due to their low-symmetry structure [13] which results in high cross-sections of the optical transitions for selected polarizations [14,15]. This leads to linearly polarized laser output [16] and depolarization losses are absent. MDTs can be doped with RE^{3+} ions with relatively high concentration without significant luminescence quenching [17] due to the relatively large RE^{3+} - RE^{3+} ion separation. The resulting short absorption lengths enable compact laser designs like the thin disk concept [18]. As it was recently shown, when cut along the special “athermal” directions [19], MDTs exhibit a positive and nearly spherical thermal lens [20,21]. This is relevant for the development of microchip lasers based on thermal guiding generating nearly-circular output beams.

In recent years, MDT microchip-type lasers based on Yb^{3+} [22], Tm^{3+} [10,23] and Ho^{3+} [24,25] ions were reported under

diode-pumping. These lasers generated multi-watt output (Yb and Tm) in the continuous-wave (CW) mode and short (even sub-ns) pulses by passive Q-switching [26,27]. However, they utilized gain crystals with low RE³⁺-doping (3-5 at.%) as used in extended cavities. Thus, the potential of RE³⁺-doped MDTs offering high transition cross-sections and high doping levels was not fully exploited. In the present paper, we aimed to prove the suitability of highly RE³⁺-doped (up to 15 at.% Tm³⁺, 10 at.% Nd³⁺ or 25 at.% Yb³⁺) MDTs for efficient laser operation in the near-IR, as well as exploit the potential for boosting the laser efficiency in the coupled ion systems (Yb³⁺-Tm³⁺ and Tm³⁺-Ho³⁺). For this, we have employed the micro-laser geometry with a plano-plano cavity and used laser-pumping to ensure proper mode-matching. As a result, record slope efficiencies for bulk MDT lasers based on Tm³⁺, Ho³⁺, Nd³⁺, and Yb³⁺ ions, as well as Yb³⁺-Tm³⁺ and Tm³⁺-Ho³⁺ ion couples are demonstrated. Consequently, this study provides a material characterization basement for the further design of efficient ultrathin *monolithic* MDT microchip lasers.

II. EXPERIMENTAL

MDTs are centrosymmetric crystals (space group $C2/c \equiv C6_{2h}$, point group $2/m$) [13]. The crystallographic b -axis coincides with the two-fold axis (C_2). The non-orthogonal a and c -axes are located in the mirror plane (m) and the angle $a \wedge c$ is 130.7° . MDTs are optically biaxial [12]. Their optical properties are described in the frame of the optical indicatrix with three principal orthogonal axes N_p , N_m and N_g (corresponding to the refractive indices, $n_p < n_m < n_g$). The N_p -axis is parallel to the b crystallographic axis. The axes corresponding to the medium and the largest refractive indices (N_m and N_g) are thus located in the a - c plane (in particular, the angle $c \wedge N_g \approx 18.5^\circ$ for KLuW).

TABLE I
IONIC RADII OF VIII-FOLD O²-COORDINATED "PASSIVE" AND "ACTIVE" IONS FOR RE³⁺-DOPED MDTs

"Passive"		"Active"	
Ion	$R, \text{\AA}$	Ion	$R, \text{\AA}$
Gd ³⁺	1.053	Nd ³⁺	1.109
Y ³⁺	1.019	Yb ³⁺	0.985
Lu ³⁺	0.977	Tm ³⁺	0.994
		Ho ³⁺	1.015

All MDT crystals studied in the present work have been grown by the Top-Seeded Solution Growth (TSSG) Slow-Cooling method using b -oriented seeds and potassium ditungstate, K₂W₂O₇, as a solvent. The choice of host-doping combination is determined by better matching of ionic radii between the "passive" Gd³⁺, Y³⁺ or Lu³⁺ ions and "active" Nd³⁺, Yb³⁺, Tm³⁺ or Ho³⁺ ions. The latter replace the "passive" ions in the same sites (C_2) with VIII-fold O²-coordination [12]. Matching of ionic radii reduces lattice distortions and, thus, minimizes passive losses in the laser elements. Table I summarizes the ionic radii of the considered "passive" and "active" ions. With respect to the best lattice matching we selected KLuW as a host for Tm and Yb doping, KYW for Ho doping and KGdW for Nd doping. The list of samples with the actual doping levels is presented in Table II.

The laser elements were polished to laser quality and remained uncoated. The Ho:KYW and Yb,Tm:KLuW samples were antireflection (AR) coated for 1.8-2.1 μm .

All studied laser samples were cut for light propagation along the N_g -axis of the optical indicatrix. This cut is chosen because of the positive sign of the thermal lens in MDT crystals with this orientation; see Table III, where the relevant parameters of thermal lens (sensitivity factor, M , astigmatism degree, S/M , and fractional heat loading, η_h) are listed, according to the previous experimental studies of Tm [10], Tm,Ho [24], Yb [22], Yb,Tm [28], Nd [29] and Ho [25] doped MDTs. In those papers, the thermal lens in the strongly anisotropic MDTs was characterized using the measurements of the divergence of the elliptic linearly polarized output laser beam and a modelling using the ray transfer matrix (ABCD) formalism [29]. The concept of the "generalized" thermo-optic coefficient [11] was also involved to predict the thermal lens parameters. The data from Table III were used for calculating the radius of the laser mode w_L in the micro-lasers. For this, we used the above-mentioned ABCD formalism. The thermal lens was considered as an ideal thin astigmatic lens located in the center of the crystal. All lasers studied in this work emitted linearly polarized radiation ($E \parallel N_m$). The polarization was naturally-selected by the anisotropy of the gain.

TABLE II
RE³⁺-DOPED MDTs USED IN THE MICRO-LASER EXPERIMENTS

Crystal	λ_p, nm	Doping	t, mm
Tm:KLuW	802	5 at.% Tm	4.0
		8 at.% Tm	2.9
		15 at.% Tm	2.5
Tm,Ho:KLuW	803	7 at.% Tm, 0.25 at.% Ho	3.0
Yb:KLuW	976	5 at.% Yb	2.6
		25 at.% Yb	0.9
Yb,Tm:KLuW	978	5 at.% Yb, 6 at.% Tm	3.0
Nd:KGdW	808	10 at.% Nd	0.9
Ho:KYW	1946	3 at.% Ho	3.0

* λ_p pump wavelength, t thickness.

TABLE III
THERMO-OPTIC PARAMETERS* OF THE STUDIED RE³⁺-DOPED MDTs**

Crystal	$\eta_h, \%$	$M, \text{m}^{-1}/\text{W}$	$S/M, \%$	Ref.
Tm:KLuW	25 \pm 5	12.9(p); 8.1(m)	37	[10]
Tm,Ho:KLuW	\sim 45	24.9(m); 24.0(p)	4	[24]
Yb:KLuW	7 \pm 1	3.5(m); 2.8(p)	20	[22]
Yb,Tm:KLuW	45 \pm 5	positive	–	[28]
Nd:KGdW	24 \pm 1	7.6(m); 7.1(p)	7	[29]
Ho:KYW	6 \pm 1	\sim 3.2(m,p)	–	[25]

* η_h – fractional heat loading; M – sensitivity factor of the thermal lens ($w_p = 100 \mu\text{m}$), S/M – astigmatism degree.

**Cut along the N_g -axis, light polarization $E \parallel N_m$.

All laser crystals were passively-cooled. They were mounted in a simple holder with a mechanical support from one side. The laser cavity was composed by a flat pump mirror (PM) and a flat output coupler (OC). Both PM and OC were placed as close as possible to the crystal minimizing air gaps. The total geometrical length of the cavity was thus equal to the thickness of the crystal. We used two sets of laser mirrors, designed for the \sim 1 and \sim 2 μm spectral ranges. For \sim 1 μm wavelength Nd and Yb lasers, the PM was AR-coated for 0.78-0.99 μm and high-reflection (HR) coated for 1.01-

1.23 μm . The OCs provided a transmission of $T_{OC} = 1\%$, 5% or 10% at 1.0-1.23 μm . They also exhibited partial reflectivity at $\sim 0.98 \mu\text{m}$ ($R \sim 85\%$), so that the pump at this wavelength double passing the active media. For $\sim 2 \mu\text{m}$ wavelength lasers, two different pump mirrors were used: PM #1, AR-coated for 0.77-1.05 μm and HR-coated for 1.8-2.08 μm , was used for the Tm, Yb-Tm and Tm-Ho lasers while the specially designed for inband-pumping of the Ho laser PM #2 was AR-coated ($T > 94\%$) for 1.9-1.99 μm and HR-coated for 2.0-2.1 μm . The OCs were specified with a transmission of $T_{OC} = 0.2\%$, 1.5% , 3% , 5% or 9% at 1.8-2 μm . However, for oscillation wavelengths $> 2 \mu\text{m}$ the exact transmission was slightly different (it will be specified in the text below). These OCs had partial reflectivity at $\sim 0.8 \mu\text{m}$ ($R \sim 35\%$) and at 1.95 μm ($R \approx 1 - T_{OC}$), resulting in a double pass pumping.

The pump absorption for each studied crystal under lasing conditions was determined from a combination of the small-signal pump-transmission measurements and a rate-equation modelling accounting for bleaching of the ground-state. The double-pass pumping geometry and the Fresnel reflections at the crystal faces were also taken into account.

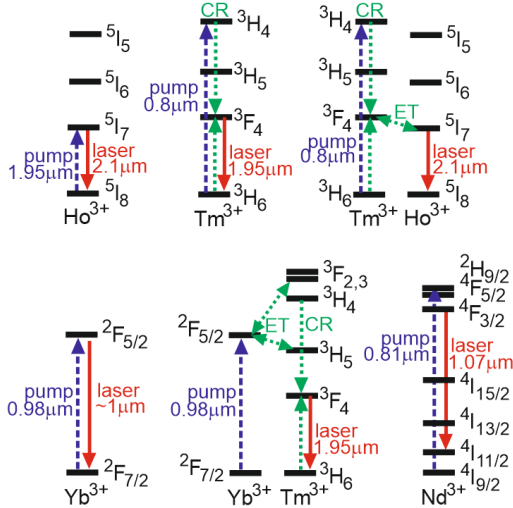


Fig. 1. Energy level schemes, pump and laser transitions and relevant interionic interactions (CR – cross-relaxation, ET – energy-transfer) for single Yb^{3+} , Nd^{3+} , Tm^{3+} and Ho^{3+} ions as well as Tm^{3+} - Ho^{3+} and Yb^{3+} - Tm^{3+} pairs.

The energy level schemes of Yb^{3+} , Nd^{3+} , Tm^{3+} , Ho^{3+} ions and Tm^{3+} - Ho^{3+} and Yb^{3+} - Tm^{3+} codoped systems are shown in Fig. 1. The relevant transitions corresponding to pump and laser emission are indicated together with the processes responsible for the excitation transfer between the active ions.

TABLE IV

ABSORPTION CHARACTERISTICS* OF THE RE^{3+} IONS IN THE STUDIED MDTs

Ion	Crystal	Transition	λ_{peak} , nm	$\Delta\lambda$, nm	σ_{abs} , 10^{-20} cm^2	Ref.
Tm^{3+}	KLuW	$^3\text{H}_6 \rightarrow ^3\text{H}_4$	801.9	4.1	5.1	[15]
Ho^{3+}	KYW	$^5\text{I}_8 \rightarrow ^5\text{I}_7$	1960.7	11.8	1.4	[30]
Yb^{3+}	KLuW	$^2\text{F}_{7/2} \rightarrow ^2\text{F}_{5/2}$	981.0	3.6	11.8	[14]
Nd^{3+}	KGdW	$^4\text{I}_{9/2} \rightarrow ^4\text{F}_{5/2} + ^2\text{H}_{9/2}$	810.5	1.7	29	[31]

* λ_{peak} – peak absorption wavelength; $\Delta\lambda$ – full width at half maximum of the absorption peak, σ_{abs} – absorption cross-section (light polarization $E \parallel N_m$).

TABLE V

EMISSION CHARACTERISTICS* OF THE RE^{3+} IONS IN THE STUDIED MDTs

Ion	Crystal	Transition	λ_{emi} , nm	σ_{SE} , 10^{-20} cm^2	τ , ms	Ref.
Tm^{3+}	KLuW	$^3\text{F}_4 \rightarrow ^3\text{H}_6$	1946	1.3	1.34	[12]
Ho^{3+}	KYW	$^5\text{I}_7 \rightarrow ^5\text{I}_8$	2075	1.2	4.80	[30]
Yb^{3+}	KLuW	$^2\text{F}_{5/2} \rightarrow ^2\text{F}_{7/2}$	1027	2.6	0.275	[14]
Nd^{3+}	KGdW	$^4\text{F}_{3/2} \rightarrow ^4\text{I}_{11/2}$	1067	21.4	0.115	[31]

* λ_{emi} – emission wavelength; σ_{SE} – stimulated-emission cross-section (light polarization $E \parallel N_m$); τ – reabsorption-free lifetime of the upper laser level.

For pumping of Yb, Nd, Tm, Yb-Tm and Tm-Ho lasers, we used a tunable Ti:Sapphire laser (Coherent MIRA 900) providing up to 1.7 W of CW output at $\sim 0.8 \mu\text{m}$ and up to 0.7 W at $\sim 0.98 \mu\text{m}$. The pump beam was focused into the crystal through the PM with a spherical lens ($f = 60 \text{ mm}$). The mean radius of the pump beam in the crystal w_p was $70 \pm 5 \mu\text{m}$. For inband-pumping of the Ho laser, we used diode-pumped Tm:KLuW laser generating up to 3 W at 1946 nm. The output of this laser was collimated and focused with a pair of lenses ($f_{\text{CL}} = 150 \text{ mm}$ and $f_{\text{FL}} = 60 \text{ mm}$) providing a w_p of $110 \pm 5 \mu\text{m}$. The output of both pump lasers corresponded to an excellent circular TEM_{00} mode with $M^2_{x,y} < 1.05$. The polarization of the pump lasers was linear and adjusted to be parallel to the N_m -axis of the laser crystal.

The absorption and emission characteristics of the RE^{3+} ions in MDTs relevant for the laser operation are listed in Table IV and Table V (for the pump and laser transitions).

III. RESULTS AND DISCUSSION

A. Thulium Micro-Lasers

Three uncoated Tm:KLuW crystals doped with 5, 8 and 15 at.% Tm have been studied. They were pumped by the Ti:Sapphire laser at 802 nm ($^3\text{H}_6 \rightarrow ^3\text{H}_4$ transition of Tm^{3+}). The laser emission corresponds to the $^3\text{F}_4 \rightarrow ^3\text{H}_6$ transition. The best output performance was achieved with the 15 at.% Tm doped crystal when using $T_{OC} = 9\%$, Fig. 2(c). The laser generated 785 mW at 1957...1965 nm (multi-peak emission arising from the etalon effects due to the small separations between the optical elements of the cavity) with a slope efficiency $\eta = 77\%$ with respect to the absorbed pump power P_{abs} . The laser threshold was at $P_{\text{abs}} = 105 \text{ mW}$. Due to the relatively high absorption in the crystal, $\sim 83\%$ (double pass pump), the optical-to-optical efficiency with respect to the incident power η_{opt} was 69%. The laser performance deteriorated at lower output coupling, with $\eta = 70, 63$ and 51% for $T_{OC} = 5\%, 3\%$ and 1.7% , respectively. In the last case, the laser threshold was as low as 55 mW.

For the $^3\text{F}_4 \rightarrow ^3\text{H}_6$ electronic transition of Tm^{3+} ions in KLuW, the longest possible emission wavelength is 1948 nm. It corresponds to the transition from the lowest Stark level of the $^3\text{F}_4$ multiplet (5663 cm^{-1}) to the highest Stark level of the $^3\text{H}_6$ multiplet (530 cm^{-1}) [15]. However, for 15 at.% Tm:KLuW, laser emission wavelengths for all OCs used were longer than 1948 nm, see Fig. 2(f). Such wavelengths are indicative of vibronic transitions [32], i.e. they occur due to the coupling with intense low-energy phonon modes of the KLuW host [33]. This effect is more pronounced for low

output coupling ($T_{OC} < 2\%$). The very low passive loss in the microchip-type cavity also facilitates multi-peak emission. For $T_{OC} = 1.7\%$ spectral emission in the range 2005...2045 nm was detected. With the increase of T_{OC} , the emission spectrum shifted to shorter wavelength which is in accordance with the gain spectra for Tm:KLuW [15] and the quasi-three level laser scheme.

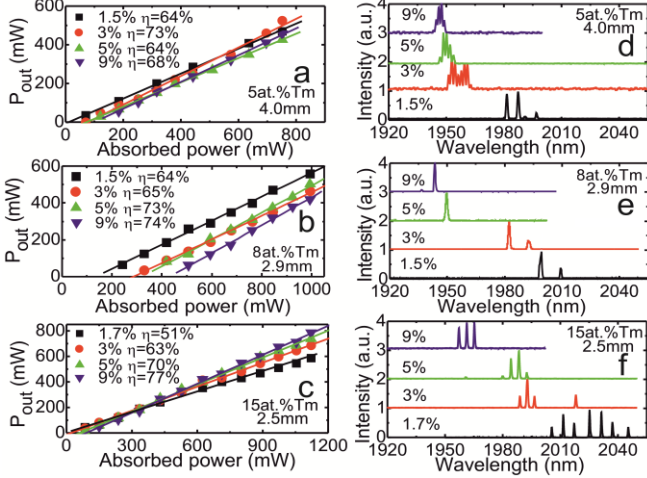


Fig. 2. Input-output dependences (a-c) and laser emission spectra at the maximum pump level (d-f) for 5, 8 and 15 at.% Tm:KLuW micro-lasers: Ti:Sapphire laser pump at 802 nm, numbers on the graphs correspond to the output coupling (T_{OC}), η is the slope efficiency.

For Tm:KLuW crystals doped with 5 and 8 at.% Tm, the maximum slope efficiencies were lower, Fig. 2(a,b). The 5 at.% Tm:KLuW laser generated 525 mW at 1950...1961 nm with $\eta = 73\%$ (for $T_{OC} = 3\%$). The laser threshold was at $P_{abs} = 80$ mW and η_{opt} was 30% mainly due to the relatively low absorption of 42% in the sample. The 8 at.% Tm:KLuW laser provided slightly higher slope efficiency, $\eta = 74\%$ with an output power of 419 mW at 1944 nm (for $T_{OC} = 9\%$). The laser threshold was at $P_{abs} = 435$ mW. In the emission spectra of both lasers, see Fig. 2(d,e), a tendency to shorter laser wavelengths is seen with the increase of T_{OC} . In this sense, by varying the doping level and output coupling, we were able to generate laser emission in the spectral range from 1944 to 2045 nm (~ 100 nm-wide). From the emission spectra of the Tm:KLuW lasers in Fig. 2(d-f) a more efficient vibronic interaction is deduced with the increase of the Tm content.

The slope efficiency of the 15 at.% Tm:KLuW micro-laser ($\eta = 77\%$) is higher compared to all previously reported bulk Tm MDT lasers and close to the record value achieved with Tm:KYW channel waveguides ($\eta = 79-82\%$) [34]. η can be expressed as:

$$\eta = \eta_{mode} \eta_{St} \eta_q \eta_{out}, \quad (1)$$

where η_{mode} is the mode-matching efficiency, $\eta_{St} = \lambda_p / \lambda_L$ is the Stokes efficiency (λ_p and λ_L are the pump and laser wavelength, respectively), η_q is the quantum efficiency of the excitation of Tm^{3+} ions (the number of emitted photons at ~ 2 μ m per one pump photon) and η_{out} is the cavity output-coupling efficiency, the relation of useful losses to total cavity

losses, $\eta_{out} = \ln[1-T_{OC}] / \ln[(1-T_{OC}) \cdot (1-L)]$ where L is the roundtrip passive loss.

The most interesting conclusion from Eq. (1) is the possibility of derivation of η_q for the highly-doped Tm:KLuW crystal. We calculated the remaining terms of η_{mode} , η_{St} and η_{out} . For a 2.5 mm-long Tm:KLuW crystal, the radius of the laser mode determined by the thermal lens is $w_L = 71 \pm 5$ μ m, which is very close to the average radius of the pump beam, $w_p = 70 \pm 5$ μ m, resulting in an excellent mode-matching ($\eta_{mode} > 0.99$). The Stokes efficiency η_{St} for 15 at.% Tm:KLuW is 0.41. The passive loss in the cavity can be estimated from the Caird plot [35], i.e. plotting the inverse of the slope efficiency vs. the inverse of the output coupling. This dependence is expressed as $1/\eta = 1/\eta_0 + (L/\eta_0) \cdot (1/T_{OC})$ where η_0 is an intrinsic slope efficiency. We estimated $L \sim 0.0071$, thus $\eta_{out} = 0.93$.

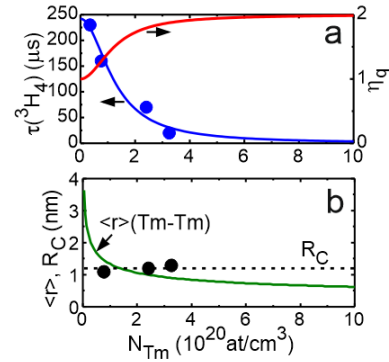


Fig. 3. (a) Lifetime of the 3H_4 state of Tm^{3+} ions in KLuW τ (symbols – experimental data from [15], curves – modelling with Eqs. (2-3), η_q : quantum efficiency of the excitation); (b) calculated average of the Tm^{3+} - Tm^{3+} distances and critical interaction range R_C (symbols – data from [15], dashed line – their average).

From Eq. (1) we determine $\eta_q = 1.98 \pm 0.02$ for 15 at.% Tm:KLuW. This means that the cross-relaxation (CR) process for two adjacent Tm^{3+} ions denoted as A and B, $^3H_4(A) + ^3H_6(B) \rightarrow ^3F_4(A) + ^3F_4(B)$ [36] is very efficient, leading to the emission of two laser photons at ~ 2 μ m after the absorption of one pump photon at ~ 0.8 μ m. To support this conclusion, we have also estimated η_q from spectroscopic data [34]:

$$\eta_q = 1 + \frac{C_{CR} N_{Tm}^2}{1/\tau_0 + C_{CR} N_{Tm}^2}. \quad (2)$$

Here, C_{CR} is the microscopic concentration-independent CR parameter, N_{Tm} is the Tm concentration and τ_0 is the intrinsic lifetime of the 3H_4 state in the absence of CR. This expression is derived under the assumption of weak ground-state bleaching. According to Eq. (2), $1 \leq \eta_q \leq 2$. Taking into account the CR effect, the lifetime of the 3H_4 state will be shortened according to [34]:

$$1/\tau = 1/\tau_0 + C_{CR} N_{Tm}^2. \quad (3)$$

By fitting the experimental data on τ [15] with this expression, see Fig. 3(a), we can estimate the value of C_{CR} as 2.7×10^{-37} cm⁶/s with $\tau_0 = 240$ μ s. Thus, the quantum efficiency of a 15

at.% Tm:KLuW crystal ($N_{\text{Tm}} = 9.8 \times 10^{20}$ at/cm³) is $\eta_q = 1.984$ which is very close to the value determined from the slope efficiency.

To complete the discussion about CR in Tm:KLuW, we have compared the averaged interionic Tm³⁺-Tm³⁺ distances, estimated as $\langle r \rangle = (4\pi N_{\text{Tm}}/3)^{-1/3}$, with the characteristic critical interaction range R_C estimated from the Inokuti-Hirayama model in [15], see Fig. 3(b). The mean value of R_C is 1.3 nm and $\langle r \rangle$ for 15 at.% Tm is only ~ 0.63 nm (comparable with the smallest Lu³⁺-Lu³⁺ separation in the KLuW lattice, 4.045 Å [12]). Thus, this crystal doping facilitates a very efficient CR.

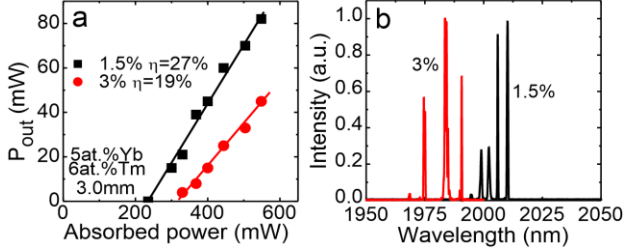


Fig. 4. Input-output characteristics of Yb,Tm:KLuW micro-laser; *inset* typical laser emission spectra. The pump is a Ti:Sapphire laser at 978 nm, the values inserted correspond to output coupling T_{OC} , η is the slope efficiency.

Another scheme for excitation of the ~ 2 μm Tm³⁺ emission is the codoping of the host with Yb³⁺ ions and pumping into $^2F_{7/2} \rightarrow ^2F_{5/2}$ absorption band of Yb³⁺ [37]. For the Yb³⁺-Tm³⁺ pair, several energy-transfer (ET) processes populate the upper laser level of Tm³⁺ (3F_4) as well as higher-lying excited states [38,39]. The latter are, however, efficiently depopulated by the CR process described above favoring the ~ 2 μm laser emission and partially suppressing unwanted up-conversion. For the laser experiment, we used a 5 at.% Yb, 6 at.% Tm:KLuW crystal, AR-coated for 1.8-2.1 μm . The crystal was pumped at 978 nm by a Ti:Sapphire laser. With $T_{\text{OC}} = 1.5\%$, this laser generated 82 mW at 1995...2010 nm with $\eta = 27\%$, Fig. 4. The laser threshold was at $P_{\text{abs}} = 235$ mW and $\eta_{\text{opt}} = 13\%$ (absorption in the crystal was 86%). For $T_{\text{OC}} = 3\%$, the slope efficiency was lower ($\eta = 19\%$) due to increased up-conversion losses and laser emission occurred at 1975...1991 nm. As in the case of Tm:KLuW, the observed long emission wavelengths in Yb,Tm:KLuW are related to vibronic coupling. As it is difficult to determine the passive losses in the Yb,Tm:KLuW crystal due to a strong impact of up-conversion, we have only estimated η_q for this crystal to be $\sim 0.7 \pm 0.1$.

B. Holmium Micro-Lasers

The simplest scheme of excitation for the Ho³⁺ ions is codoping with Tm³⁺ ions [40]. Tm ions pumped at 0.8 μm ($^3H_6 \rightarrow ^3H_4$ transition) transfer efficiently the excitation to the 3F_4 state due to the CR process. As the 3F_4 state of Tm³⁺ and the 5I_7 state of Ho³⁺ are almost resonant in energy and the barycenter of the 3F_4 multiplet is lying slightly higher than that of the 5I_7 one, efficient and predominantly unidirectional Tm³⁺ \rightarrow Ho³⁺ ET may occur, followed by the desired $^5I_7 \rightarrow ^5I_8$ Ho³⁺ emission at ~ 2 μm . Indeed, the position of the barycenters for Tm³⁺ and Ho³⁺ ions in KLuW are 5851 cm⁻¹

and 5187 cm⁻¹, respectively, and the ratio of the microparameters that account for Ho \rightarrow Tm and Tm \rightarrow Ho ETs for Tm,Ho-codoped KLuW, called equilibrium constant Θ , equals 0.089 ± 0.003 [41]. For Tm,Ho:KLuW, the combination of high Tm concentration and high Tm/Ho codoping ratio (typically from 5:1 to 10:1) provides efficient Tm absorption, high ET probability and low up-conversion losses.

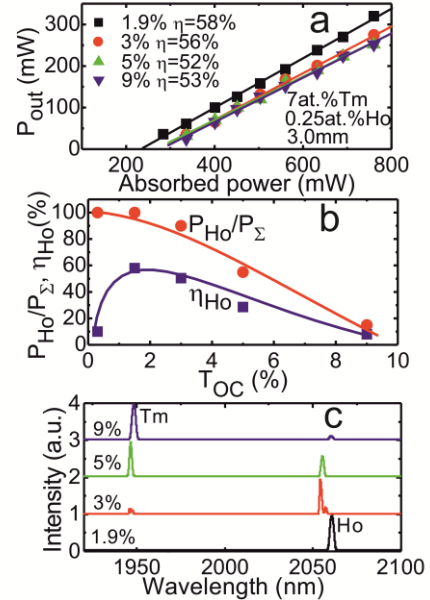


Fig. 5. 7 at.% Tm, 0.25 at.% Ho:KLuW micro-laser (a) Input-output dependences; (b) fraction of Ho emission with respect to the total emitted power P_{Ho}/P_{Σ} and slope efficiency for the Ho emission η_{Ho} vs. output coupling (T_{OC}); (c) laser emission spectra at the maximum pump level. The pump source is a Ti:Sapphire laser at 803 nm, numbers on the graphs in (a) and (c) correspond to T_{OC} , η is the total slope efficiency.

For these reasons, we selected a 7 at.% Tm, 0.25 at.% Ho:KLuW crystal for the laser experiments. The crystal was uncoated. It was pumped at 803 nm by a Ti:Sapphire laser. The best output performance was observed with $T_{\text{OC}} = 1.9\%$, Fig. 5(a), which is attributed to the reduction of up-conversion loss due to low population inversion [24]. The Tm,Ho:KLuW micro-laser generated 320 mW with $\eta_{\text{Ho}} = 58\%$ at 2061 nm (pure Ho emission). The laser threshold was at $P_{\text{abs}} = 240$ mW. The optical-to-optical efficiency was 22% (with respect to the incident pump power) which was limited by the 52% crystal absorption. For higher T_{OC} , the laser performance deteriorated and Tm,Ho colasing [42] was observed. Moreover, the fraction of Ho emission with respect to the total output power P_{Ho}/P_{Σ} decreased with the increase of T_{OC} , from >0.99 for the 1.5...1.9% OC to 0.15 for the 9% OC, Fig. 5(b). This reduction correlates with the drop of the slope efficiency of pure Ho emission, η_{Ho} , to 8% for $T_{\text{OC}} = 9\%$ while the drop in the total slope efficiency was less profound ($\eta = 53\%$). Tm³⁺ emission was detected at 1947-1948 nm and Ho³⁺ ions emitted at 2055-2061 nm, Fig. 5(c), with weak dependence of the emission wavelengths on the output coupling.

With Eq. (1), we have also estimated the quantum efficiency η_q for Tm³⁺,Ho³⁺ codoped KLuW. Due to the strong thermal lens related to high heat load in Tm,Ho:KLuW (cf. Table III), the radius of the laser mode in the crystal w_L

was $68 \pm 5 \mu\text{m}$, so $\eta_{\text{mode}} > 0.98$. The Stokes efficiency η_{st} was 0.39 ($\lambda_{\text{p}} = 803 \text{ nm}$ and $\lambda_{\text{L}} = 2061 \text{ nm}$). Assuming the intrinsic loss to be slightly lower than that of Tm:KLuW due to lower doping ($L \approx 6 \times 10^{-3}$), η_{out} amounted to 0.76. Finally, η_{q} was found to be 1.95 ± 0.02 (at low inversion ratios). However, at high inversion ratios, the ${}^3\text{F}_4$ state was mainly depopulated by the Tm $^{3+}$ emission but not by Tm \rightarrow Ho ET and Ho emission. This can be explained as follows: Although at thermodynamical equilibrium the fractional populations of Tm $^{3+}$ and Ho $^{3+}$ ions in their upper laser levels (${}^3\text{F}_4$ and ${}^5\text{I}_7$, respectively) are $f_{\text{Tm}} \approx 30\%$ and $f_{\text{Ho}} \approx 70\%$ for Tm,Ho:KLuW [41], the gain cross-sections σ_{g} at the corresponding laser wavelengths are higher for Tm $^{3+}$ than for Ho $^{3+}$ [15,43], consequently, at a certain level of inversion both Tm $^{3+}$ and Ho $^{3+}$ emission is possible.

Another way of excitation of the Ho $^{3+}$ ions is their resonant (in-band) pumping to the ${}^5\text{I}_7$ upper laser level [44], i.e. by a Tm laser. This scheme provides high laser slope efficiencies due to the low quantum defect and almost vanishing up-conversion. For laser experiments, a 3 at.% Ho:KYW crystal AR-coated for 1.8-2.1 μm was employed. It was pumped at 1946 nm by a Tm:KLuW laser. With $T_{\text{OC}} = 0.5\%$, the Ho:KYW laser generated 206 mW at 2100 ...2105 nm with $\eta = 85\%$, see Fig. 6. The laser threshold was at $P_{\text{abs}} = 190 \text{ mW}$ and the optical-to-optical efficiency (with respect to the incident power) amounted to 13%, limited mainly by the low absorption of the Ho crystal, 26%. For $T_{\text{OC}} = 2.1\%$, the laser performance was slightly inferior, with an output power of 161 mW at 2077...2079 nm and $\eta = 79\%$.

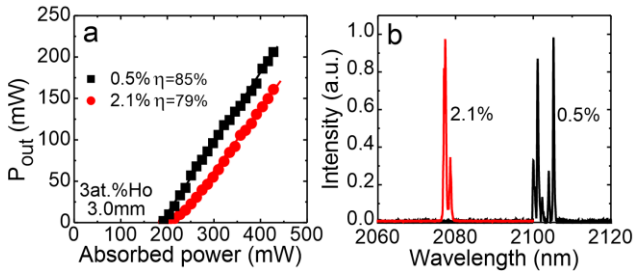


Fig. 6. Input-output characteristics of the 3 at.% Ho:KYW micro-laser; inset typical laser emission spectra. The pump source is a Tm:KLuW laser at 1946 nm, numbers correspond to T_{OC} , η is the slope efficiency.

The radii of the pump and laser beams for the Ho:KYW laser were calculated to be $w_{\text{p}} \approx w_{\text{L}} = 110 \pm 5 \mu\text{m}$, meaning $\eta_{\text{mode}} > 0.99$. The Stokes efficiency for this laser was $\eta_{\text{st}} = 0.93$ ($\lambda_{\text{p}} = 1946 \text{ nm}$ and $\langle \lambda_{\text{L}} \rangle = 2102 \text{ nm}$). The output-coupling efficiency was determined as $\eta_{\text{out}} = 0.96$ assuming $L \approx 0.2 \times 10^{-3}$. The losses were estimated from the background absorption of the MDTs measured by laser calorimetry in their transparency range (unpublished data) and considering the AR-coatings on both crystal faces. Thus, $\eta_{\text{q}} > 0.99$ which is consistent with the five times larger energy gap between the lowest Stark level of the ${}^5\text{I}_7$ state of Ho $^{3+}$ in KYW (5100 cm^{-1}) and highest level of the ${}^5\text{I}_8$ ground-state (281 cm^{-1}) than the maximum phonon frequency of the host ($\nu_{\text{max}} = 907 \text{ cm}^{-1}$) leading to almost vanishing non-radiative relaxation probability from this multiplet.

C. Ytterbium Micro-Lasers

We studied two Yb:KLuW crystals, doped with 5 and 25 at.% Yb. The uncoated crystals have thicknesses of 2.6 and 0.9 mm, respectively. They were pumped at 976 nm by a Ti:Sapphire laser (${}^2\text{F}_{7/2} \rightarrow {}^2\text{F}_{5/2}$ transition of Yb $^{3+}$). The highly-doped Yb:KLuW crystal generated 308 mW at 1059...1061 nm (${}^2\text{F}_{5/2} \rightarrow {}^2\text{F}_{7/2}$ transition) with a slope efficiency of 91% for $T_{\text{OC}} = 5\%$, Fig. 7(b,d). The laser threshold was at $P_{\text{abs}} = 90 \text{ mW}$ and the optical-to-optical efficiency amounted to 41% (as the absorption in the crystal was 54%). For $T_{\text{OC}} = 1\%$ and 10%, the laser performance was slightly inferior, however, still with very high slope efficiency. With the increase of the output coupling, the laser wavelength shortened from 1084...1086 nm (for $T_{\text{OC}} = 1\%$) to 1043...1046 nm (for $T_{\text{OC}} = 10\%$), Fig. 7(d), in accordance with the gain curves for Yb:KLuW [14].

The performance of the 5 at.% Yb:KLuW crystal was inferior, with a maximum extracted output power of 201 mW at 1943...1946 nm corresponding to $\eta = 83\%$ (for $T_{\text{OC}} = 5\%$), Fig. 7(a,c). The shorter laser wavelengths, higher threshold ($P_{\text{abs}} = 160 \text{ mW}$) and lower optical-to-optical efficiency ($\eta_{\text{opt}} = 29\%$) were mainly due to higher internal losses in the longer (2.6 mm) crystal.

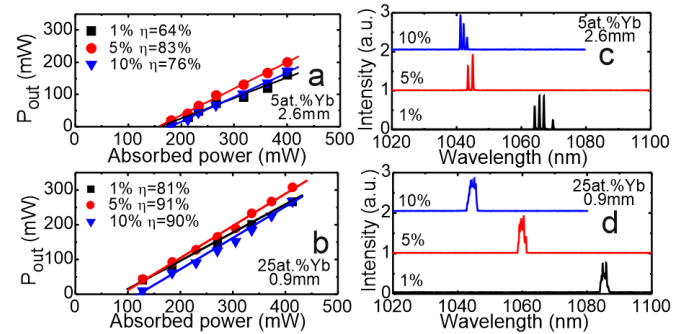


Fig. 7. Input-output characteristics (a,b) and laser emission spectra (c,d) for the 5 and 25 at.% Yb:KLuW micro-lasers. The pump source is a Ti:Sapphire laser at 976 nm, the numbers on the graphs correspond to the output coupling (T_{OC}), η is the slope efficiency.

For the Yb $^{3+}$ ion in KLuW, the energy gap between the lowest Stark level of the ${}^2\text{F}_{5/2}$ excited-state and the highest Stark level of the ${}^2\text{F}_{7/2}$ ground-state (9628 cm^{-1}) is ~ 9 times larger than the maximum phonon frequency of the host. Consequently, one can expect η_{q} to approach unity. Thus, the conditions of good mode-matching ($w_{\text{p}} = 69 \pm 5 \mu\text{m}$, $w_{\text{L}} = 70 \pm 5 \mu\text{m}$) and low passive losses were satisfied for the 0.90-mm-thin 25 at.% Yb-doped crystal. The Stokes efficiency of the laser amounted to $\eta_{\text{st}} = 0.92$ ($\lambda_{\text{p}} = 978 \text{ nm}$ and $\langle \lambda_{\text{L}} \rangle = 1060 \text{ nm}$) and it is the main factor that determines the slope efficiency η which approached the theoretical limit in the case of the highly-doped Yb:MDT micro-laser.

D. Neodymium Micro-Lasers

The typical doping concentration for Nd in KGdW is 3 at.%. However, doping of this crystal with up to ~ 10 at.% Nd is possible keeping the desirable monoclinic phase, still at relatively low optical losses. For the laser experiment, we have used a 0.9-mm-thick 10 at.% Nd:KGdW crystal. The

uncoated sample was pumped by a Ti:Sapphire laser at 808 nm ($^4I_{9/2} \rightarrow ^4F_{5/2} + ^2H_{9/2}$ transition of Nd^{3+}).

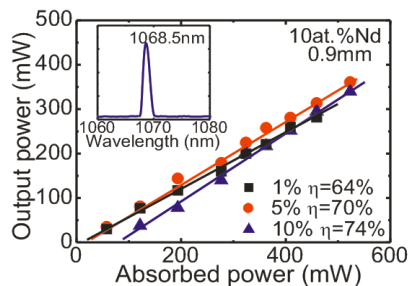


Fig. 8. Input-output characteristics of the 10 at.% Nd:KGdW micro-laser. The pump source is a Ti:Sapphire laser at 808 nm, numbers on the graph correspond to the output coupling (T_{OC}), η is the slope efficiency, inset typical laser spectrum.

With $T_{OC} = 10\%$, the maximum output power was 340 mW at 1068 nm ($^4F_{3/2} \rightarrow ^4I_{11/2}$ transition) corresponding to $\eta = 74\%$, Fig. 8. The laser threshold was at $P_{abs} = 80$ mW and $\eta_{opt} = 25\%$. The latter value was limited mainly by the low absorption in the crystal (39%) required to avoid thermal fracture under passive cooling conditions. With the decrease of T_{OC} , the slope efficiency dropped while the emission wavelength remained almost unchanged which is typical for 4-level Nd^{3+} lasers. For low output coupling, the laser threshold of the Nd:KGdW micro-laser was as low as 25 mW. The use of a thin crystal provided good mode-matching ($w_p = 70 \pm 5$ μm and $w_L = 66 \pm 5$ μm , so $\eta_{mode} = 0.94$) and relatively low losses ($L = 1.5 \times 10^{-3}$, as estimated from the Caird plot, see above, so $\eta_{out} = 0.99$). As a consequence, the quantum efficiency for Nd^{3+} in KGdW is $\eta_q > 0.98$.

E. Discussion

As already mentioned, at ~ 2 μm , the achieved slope efficiencies of the different Tm:KLuW micro-lasers ($\eta > 70\%$) is superior compared to the previously reported Tm-doped MDT micro- and bulk lasers and the best value $\eta = 77\%$ is close to the record value for Tm:KYW waveguide lasers ($\eta = 79-82\%$) [34]. This is due to very efficient CR for highly-doped (15 at.% Tm) crystal, as expressed by the quantum efficiency η_q almost approaching its theoretical limit of 2, as well as low losses and good mode-matching in the microchip-type set-up. We have also achieved high optical-to-optical conversion efficiency with respect to the incident power ($\eta_{opt} = 69\%$), almost 1.5 times higher than in previous reports [23]. Further work on Tm lasers shall be focused on further increase of the Tm doping level and reduction of cavity length to few hundreds of μm .

A significant improvement is demonstrated also for the Tm-Ho laser by increasing the Tm doping and Tm/Ho codoping ratio (28:1) which helped to increase the maximum slope efficiency of the Tm,Ho:KLuW micro-laser by a factor of ~ 2 ($\eta = 58\%$) with respect to a previous work [24] and prevent Tm/Ho colasing [42]. This indicates the possibility of efficient laser operation at ~ 2.1 μm in properly codoped Tm-Ho MDT waveguide lasers which have not been reported to date. For the in-band-pumped Ho laser, our results with Ho:KYW are similar to those for Ho:KLuW [25] still showing relatively

low optical-to-optical efficiency ($\eta_{opt} = 13\%$) due to the weak absorption of Ho^{3+} ions. Thus, studies of highly-doped crystals, as well as pump sources emitting around 1961 nm are required.

For the Yb-Tm laser, although we have achieved the highest value of slope efficiency ever reported for this type of lasers ($\eta = 27\%$), further improvement of the Yb/Tm codoping ratio is required in order to suppress or minimize up-conversion losses.

At ~ 1 μm , the most significant achievement is the highly-efficient micro-laser operation ($\eta = 91\%$) with a passively-cooled highly-doped sub-mm thick 25 at.% Yb:KLuW crystal. The achieved slope efficiency is higher compared to previous reports of a Yb:KYW waveguide laser [45] and a Yb:KLuW bulk laser [12] ($\eta = 78\%$ for both lasers). This record value confirms the potential of highly Yb-doped MDTs for ultrathin highly efficient lasers, questioned after a previous work with 250 μm -thin 10 at.% Yb:KYW diamond-bonded microchip laser [46] and stoichiometric KYbW [17] both showing a η limited to 41%. Although we have achieved reasonable optical-to-optical efficiency in the 25 at.% Yb:KLuW laser ($\eta_{opt} = 41\%$) it can be further improved by optimizing the doping and thickness of the sample.

With the Nd laser, we successfully tested the laser operation of 10 at.% Nd:KGdW which almost corresponds to the stability limit of the monoclinic phase. The achieved slope efficiency ($\eta = 74\%$) is approaching the theoretical limit for this type of lasers and it is comparable with the best bulk Nd:KGdW lasers containing conventional Nd-doping levels of about 3 at.% [47]. Future work on Nd:KGdW shall be focused on in-band-pumping of Nd^{3+} ions into the $^4F_{3/2}$ upper laser level at ~ 0.88 μm which could lead to $\eta > 80\%$ as well as better heat management. Other laser transitions of Nd^{3+} ions in KGdW at ~ 0.91 and 1.35 μm may be studied as well.

Efficient vibronic laser operation with highly Tm-doped MDTs indicates the potential of these materials for CW vibronic lasers emitting above 2 μm with a proper wavelength-selective manipulation of losses in the laser cavity [48]. CW self-Raman conversion in MDTs has been realized only at ~ 1 μm with Nd^{3+} doping [49] and the poor thermo-optic behavior of the material (Nd:KGdW) was identified as the main limitation for power scaling. As highly Tm $^{3+}$ -doped MDTs exhibit very efficient CR, heat loading can be even lower as compared with Nd lasers. Vibronic Tm lasers can compete with the Tm,Ho ones suffering from up-conversion losses [50].

Previously, it was experimentally demonstrated that Yb and Tm microchip-type MDT lasers generated sub-ns pulses when passively Q-switched by "slow" SAs, namely Cr:YAG and Cr:ZnS, respectively [26,51]. The suitability of RE $^{3+}$ -doped MDTs showing high stimulated-emission cross-sections for this type of lasers was also confirmed by numerical modelling. In [26,27,51], relatively long (few mm) and low-doped crystals were used. The results achieved in the present paper with highly-doped MDTs together with the above-mentioned modelling indicates that the concept of ultrathin highly-doped Yb and Tm microchips is promising for generation of sub-ns and even sub-100 ps high-energy pulses at pulse repetition frequencies of few kHz when inserting

“slow” SAs such as Cr:YAG [7,8] or V:YAG (for Yb) and Cr:ZnS or Cr:ZnSe [26] (Tm) into the cavity. They are also attractive for the generation of few-ns pulses at high repetition frequencies (potentially reaching MHz range) with carbon nanostructures, e.g., graphene, single-walled carbon nanotubes [48], deposited directly on the crystal face and thus keeping very short cavity length and preventing high insertion loss for the absorber. In this case, the microchip set-up can ensure the high peak intracavity intensities on the saturable absorber (few MW/cm²) needed for its saturation.

The results achieved in this work related to the laser characteristics are summarized in Table VI where the previously reported maximum slope efficiencies are also included for comparison.

IV. CONCLUSION

We report on a detailed study of MDTs singly-doped with the RE³⁺ ions in high concentrations (up to 15 at.% of Tm³⁺, 10 at.% of Nd³⁺ and 25 at.% of Yb³⁺), and codoped with the Tm³⁺-Ho³⁺ and Yb³⁺-Tm³⁺ ion couples, for the development of highly-efficient micro-lasers emitting at ~1 μm and at ~2 μm. The unique structural and spectroscopic properties of MDTs (high transition cross-sections in polarized light, intense and broad spectral bands for the RE³⁺ ions and high accessible doping levels due to the long interionic distances), as well as proper managing of their thermo-optic behavior by a special nearly-athermal cut determine the suitability of these materials for sub-mm thick, efficient passively-cooled CW microchip lasers and to further development of short-pulse (hundreds of ps) passively Q-switched oscillators. Using a compact micro-laser design and a laser-pumping, we demonstrate the record slope efficiencies for bulk RE³⁺ MDT lasers for all considered ions and ion couples.

In particular, in the eye-safe 2 μm spectral range, the 15 at.% Tm:KLuW laser generated 785 mW at 1957...1965 nm with a slope efficiency $\eta = 77\%$ (with respect to the absorbed power) and $\eta_{opt} = 69\%$. The high efficiency is attributed to the efficient CR in this crystal, with the quantum efficiency for Tm³⁺ ions amounting to $\eta_q = 1.98 \pm 0.02$. In addition, vibronic laser emission at wavelengths as long as 2005...2045 nm is achieved from the Tm-laser, that is the first step towards CW Tm vibronic lasers operating at > 2 μm. For the Tm³⁺-Ho³⁺ ion couple, we proved that high Tm doping and Tm/Ho codoping ratio are the key factors for the ultimate improvement of the laser slope efficiency ($\eta = 58\%$). This observation is useful for the design of waveguide lasers of this type.

REFERENCES

- [1] J. J. Zayhowski, “Microchip lasers,” *Opt. Mater.*, vol. 11, pp. 255-267 (1999).
- [2] J. J. Zayhowski and C. Dill III, “Diode-pumped passively Q-switched picosecond microchip lasers,” *Opt. Lett.*, vol. 19, pp. 1427-1429 (1994).
- [3] S. Forget *et al.*, “Passively Q-switched diode-pumped Cr⁴⁺:YAG / Nd³⁺:GdVO₄ monolithic microchip laser,” *Opt. Commun.*, vol. 259, pp. 816-819 (2006).
- [4] C.P. Wyss *et al.*, “Emission properties of a 0.1 mm Tm³⁺:GdVO₄ microchip laser at 1.9 μm,” *Appl. Phys. B*, vol. 67, pp. 545-548 (1998).
- [5] J. J. Zayhowski, J. Harrison, C. Dill, and J. Ochoa, “Tm:YVO₄ microchip laser,” *Appl. Opt.*, vol. 34, pp. 435-437 (1995).
- [6] A. C. Butler, D. J. Spence, and D. W. Coutts, “Scaling Q-switched microchip lasers for shortest pulses,” *Appl. Phys. B*, vol. 109, pp. 81-88 (2012).
- [7] J. Dong, A. Shirakawa, and K. Ueda, “Sub-nanosecond passively Q-switched Yb:YAG / Cr⁴⁺:YAG sandwiched microchip laser,” *Appl. Phys. B*, vol. 85, pp. 513-518 (2006).
- [8] J. Dong, K. Ueda, A. Shirakawa, H. Yagi, T. Yanagitani, and A. A. Kaminskii, “Composite Yb:YAG / Cr⁴⁺:YAG ceramics picosecond microchip lasers,” *Opt. Express*, vol. 15, pp. 14516-14523 (2007).
- [9] N. Hodgson, H. Weber, *Optical resonators: fundamentals, advanced concepts and applications* (Springer, London, 1997).
- [10] J. M. Serres *et al.*, “Diode-pumped microchip Tm:KLu(WO₄)₂ laser with more than 3 W of output power,” *Opt. Lett.*, vol. 39, pp. 4247-4250 (2014).
- [11] S. Chenais, F. Druon, S. Forget, F. Balembos, and P. Georges, “On thermal effects in solid-state lasers: The case of ytterbium-doped materials,” *Progress in Quant. Electron.*, vol. 30, pp. 89-153 (2006).
- [12] V. Petrov *et al.*, Growth and properties of KLu(WO₄)₂, and novel ytterbium and thulium lasers based on this monoclinic crystalline host, *Laser & Photon. Rev.*, vol. 1, pp. 179-212 (2007).
- [13] M.C. Pujol *et al.*, “Structural study of monoclinic KGd(WO₄)₂ and effects of lanthanide substitution,” *J. Appl. Crystallogr.*, vol. 34, pp. 1-6 (2001).
- [14] X. Mateos *et al.*, “Crystal growth, spectroscopic studies and laser operation of Yb³⁺-doped potassium lutetium tungstate,” *Opt. Mater.*, vol. 28, pp. 519-523 (2006).
- [15] O. Silvestre, M.C. Pujol, M. Rico, F. Güell, M. Aguiló, and F. Díaz, “Thulium doped monoclinic KLu(WO₄)₂ single crystals: growth and spectroscopy,” *Appl. Phys. B* 87, 707-716 (2007).
- [16] J. Liu, V. Petrov, X. Mateos, H. Zhang, and J. Wang, “Efficient high-power laser operation of Yb:KLu(WO₄)₂ crystals cut along the principal optical axes,” *Opt. Lett.*, vol. 32, pp. 2016-2018 (2007).
- [17] M.C. Pujol *et al.*, “Growth, optical characterization, and laser operation of a stoichiometric crystal KYb(WO₄)₂,” *Phys. Rev. B*, vol. 65, pp. 165121-1-11 (2002).
- [18] S. Vatik *et al.*, “Efficient thin-disk Tm-laser operation based on Tm:KLu(WO₄)₂/KLu(WO₄)₂ epitaxies,” *Opt. Lett.*, vol. 37, pp. 356-358 (2012).
- [19] S. Biswal, S. P. O’Connor, and S. R. Bowman, “Thermo-optical parameters measured in ytterbium-doped potassium gadolinium tungstate,” *Appl. Opt.*, vol. 44, pp. 3093-3097 (2005).
- [20] F. Hoos, S. Li, T.P. Meyrath, B. Braun, and H. Giessen, “Thermal lensing in an end-pumped Yb:KGW slab laser with high power single emitter diodes,” *Opt. Express*, vol. 16, pp. 6041-6049 (2008).
- [21] M. S. Gaponenko, P. A. Loiko, N. V. Gusakova, K. V. Yumashev, N. V. Kuleshov, and A. A. Pavlyuk, “Thermal lensing and microchip laser performance of N_g-cut Tm³⁺:KY(WO₄)₂ crystal,” *Appl. Phys. B*, vol. 108,

TABLE VI

OUTPUT PERFORMANCE OF THE MICRO-LASERS BASED ON RE³⁺-DOPED MDTs SHOWING RECORD SLOPE EFFICIENCIES

Ion	Crystal	λ_L , nm	P_{th} , mW	P_{out} , mW	η , %	η_{opt} , %	η_q	η_{REF}
Tm	KLuW	1957...1965	105	785	77	69	1.98±0.02	71 [23]
Tm-Ho	KLuW	2061	240	320	58	22	1.95±0.02	31 [24]
Yb	KLuW	1059...1061	90	308	91	41	>0.99	65 [22]
Yb-Tm	KLuW	1995...2010	235	82	27	13	~0.7±0.1	20 [28]
Nd	KGdW	1068	80	340	74	25	>0.98	33 [46]
Ho	KYW	2100...2105	190	206	85	13	>0.99	84 [25]

* λ_L – wavelength of laser emission; P_{th} – laser threshold, P_{out} – maximum output power, η – slope efficiency, η_{REF} – maximum slope efficiency reported in the literature for MDT micro-laser (both with respect to the absorbed power), η_{opt} – optical-to-optical efficiency (with respect to the incident power), η_q – quantum efficiency.

- pp. 603-607 (2012).
- [22] J.M. Serres *et al.*, "Prospects of monoclinic Yb:KLu(WO₄)₂ crystal for multi-watt microchip lasers," *Opt. Mater. Express*, vol. 5, pp. 661-667 (2015).
- [23] M. Gaponenko, N. Kuleshov, and T. Südmeyer, "Efficient diode-pumped Tm:KYW 1.9- μm microchip laser with 1 W cw output power," *Opt. Express*, vol. 22, pp. 11578-11582 (2014).
- [24] P. Loiko *et al.*, "Microchip laser operation of Tm,Ho:KLu(WO₄)₂ crystal," *Opt. Express*, vol. 22, pp. 27976-27984 (2014).
- [25] P. Loiko *et al.*, "In-band-pumped Ho:KLu(WO₄)₂ microchip laser with 84% slope efficiency," *Opt. Lett.* 40, 344-347 (2015).
- [26] P. Loiko *et al.*, "Subnanosecond Tm:KLuW microchip laser Q-switched by a Cr:ZnS saturable absorber," *Opt. Lett.*, vol. 40, pp. 5220-5223 (2015).
- [27] M. Gaponenko, N. Kuleshov, and T. Südmeyer, "Passively Q-switched Thulium microchip laser," *IEEE Photon. Technol. Lett.*, vol. 28, pp. 147-150 (2016).
- [28] P. A. Loiko *et al.*, "Spectroscopic and laser characterization of Yb,Tm:KLu(WO₄)₂ crystal," *Opt. Mater.*, vol. 51, pp. 223-231 (2016).
- [29] P. A. Loiko, V. G. Savitski, A. Kemp, A. A. Pavlyuk, N. V. Kuleshov, and K. V. Yumashev, "Anisotropy of the photo-elastic effect in Nd:KGd(WO₄)₂ laser crystals," *Laser Phys. Lett.*, vol. 11, pp. 055002-1-7 (2014).
- [30] A. A. Lagatsky *et al.*, "Optical spectroscopy and efficient continuous-wave operation near 2 μm for a Tm, Ho:KYW laser crystal," *Appl. Phys. B*, vol. 97, pp. 321-326 (2009).
- [31] P. Loiko *et al.*, "Temperature-dependent spectroscopy and microchip laser operation of Nd:KGd(WO₄)₂," *Opt. Mater.*, vol. 58, pp. 365-372 (2016).
- [32] F. Cornacchia, D. Parisi, C. Bernardini, A. Toncelli, and M. Tonelli, "Efficient, diode-pumped Tm³⁺:BaY₂F₈ vibronic laser," *Opt. Express*, vol. 12, pp. 1982-1989 (2004).
- [33] M. Segura *et al.*, "Diode-pumped 2 μm vibronic (Tm³⁺, Yb³⁺):KLu(WO₄)₂ laser," *Appl. Opt.*, vol. 51, pp. 2701-2705 (2012).
- [34] K. van Dalfsen, S. Aravazhi, C. Grivas, S. M. García-Blanco, and M. Pollnau, "Thulium channel waveguide laser with 1.6 W of output power and ~80% slope efficiency," *Opt. Lett.*, vol. 39, pp. 4380-4383 (2014).
- [35] J. A. Caird, S. A. Payne, P. R. Staber, A. J. Ramponi, L. L. Chase, and W. F. Krupke, "Quantum electronic properties of the Na₃Ga₂Li₃F₁₂:Cr³⁺ laser," *IEEE J. Quantum Electron.*, vol. 24, pp. 1077-1099 (1988).
- [36] P. Loiko, and M. Pollnau, "Stochastic model of energy-transfer processes among rare-earth ions. Example of Al₂O₃:Tm³⁺," *J. Phys. Chem. C*, vol. 120, pp. 26480-26489 (2016).
- [37] E. Batay, A. A. Demidovich, A. N. Kuzmin, A. N. Titov, M. Mond, and S. Kück, "Efficient tunable laser operation of diode pumped Yb,Tm:KY(WO₄)₂ around 1.9 μm ," *Appl. Phys. B*, vol. 75, pp. 457-461 (2002).
- [38] B. Peng, and T. Izumitani, "Optical properties, fluorescence mechanisms and energy transfer in Tm³⁺, Ho³⁺ and Tm³⁺-Ho³⁺ doped near-infrared laser glasses, sensitized by Yb³⁺," *Opt. Mater.*, vol. 4, pp. 797-810 (1995).
- [39] K. Li, Q. Zhang, G. Bai, S. Fan, J. Zhang, and L. Hu, "Energy transfer and 1.8 μm emission in Tm³⁺/Yb³⁺ codoped lanthanum tungsten tellurite glasses," *J. Alloys Compd.*, vol. 504, pp. 573-578 (2010).
- [40] T. Y. Fan, G. Huber, R. L. Byer, and P. Mitzscherlich, "Spectroscopy and diode laser-pumped operation of Tm,Ho:YAG," *IEEE J. Quantum Electron.*, vol. 24, pp. 924-933 (1988).
- [41] J. M. Serres *et al.*, "Q-switching of Tm,Ho:KLu(WO₄)₂ microchip laser by a graphene-based saturable absorber," *Laser Phys. Lett.*, vol. 13, pp. 025801-1-5 (2016).
- [42] V. Jambunathan *et al.*, "Continuous-wave co-lasing in a monoclinic co-doped (Ho,Tm): KLu(WO₄)₂ crystal," *Laser Phys. Lett.*, vol. 8, pp. 799-803 (2011).
- [43] V. Jambunathan *et al.*, "Crystal growth, optical spectroscopy, and continuous-wave laser operation of Ho:KLu(WO₄)₂ crystals," *Appl. Phys. B*, vol. 116, pp. 455-466 (2014).
- [44] P. A. Budni, M. L. Lemons, J. R. Mosto, and E P. Chicklis, "High-power/high-brightness diode-pumped 1.9- μm thulium and resonantly pumped 2.1- μm holmium lasers," *IEEE J. Sel Top. Quantum Electron.*, vol. 6, pp. 629-635 (2000).
- [45] D. Geskus *et al.*, "Low-threshold, highly efficient Gd³⁺, Lu³⁺ co-doped KY(WO₄)₂: Yb³⁺ planar waveguide lasers," *Laser Phys. Lett.*, vol. 6, pp. 800-805 (2009).
- [46] V. G. Savitski *et al.*, "The prospects for Yb- and Nd-doped tungstate microchip lasers," in CLEO/Europe-EQEC 2013, Munich, May, 12-16, 2013, P. CA-10.5.
- [47] A. Abdolvand, K. G. Wilcox, T. K. Kalkandjiev, and E. U. Rafailov, "Conical refraction Nd:KGd(WO₄)₂ laser," *Opt. Express*, vol. 18, pp. 2753-2759 (2010).
- [48] P. Loiko *et al.*, "Vibronic thulium laser at 2131 nm Q-switched by single-walled carbon nanotubes," *J. Opt. Soc. Am. B.*, vol. 33, pp. D19-D27 (2016).
- [49] A. A. Demidovich, A. S. Grabtchikov, V. A. Lisinetskii, V. N. Burakevich, V. A. Orlovich, and W. Kiefer, "Continuous-wave Raman generation in a diode-pumped Nd³⁺:KGd(WO₄)₂ laser," *Opt. Lett.*, vol. 30, pp. 1701-1703 (2005).
- [50] P. Loiko *et al.*, "Comparative spectroscopic and thermo-optic study of Tm:LiLnF₄ (Ln = Y, Gd, and Lu) crystals for highly-efficient microchip lasers at ~2 μm ," *Opt. Mater. Express*, vol. 7, pp. 844-854 (2017).
- [51] P. Loiko *et al.*, "Sub-nanosecond Yb:KLu(WO₄)₂ microchip laser," *Opt. Lett.*, vol.41, pp. 2620-2623 (2016).